International Journal of Power Electronics and Drive System (IJPEDS)
Vol. 17, No. 4, December 2026, pp. 3062~3074
ISSN: 2088-8694, DOI: 10.11591/ijpeds.v17.i4.pp3062-3074

Spectral machine learning framework for power system contingency assessment

Yusri Ambabunga, Indar Chaerah Gunadin, Yusri Syam Akil, Zaenab Muslimin
Department of Electrical Engineering, Faculty of Engineering, Universitas Hasanuddin, Makassar, Indonesia

Article Info

Article history:

Received Feb 13, 2026
Revised Sep 7, 2026
Accepted Sep 17, 2026

Keywords:

AC/DC power flow
Fast Fourier transform
Power system contingency
Renewable energy integration
Support vector machine

ABSTRACT

This study proposes a fast static-security screening framework for contingency assessment in renewable-integrated power systems. The IEEE 118-bus system is modified by adding a 50 MW photovoltaic unit and an 80 MW wind generator. The framework combines DC load-flow-based N-1/N-2 screening, AC power-flow validation, fast Fourier transform (FFT) spatial spectral feature extraction, and support vector machine (SVM) classification. The DC model is used as a preliminary screening engine rather than a full substitute for AC power flow, and its limitations are evaluated through case-by-case AC/DC validation, line-resistance sensitivity, and reactive-load sensitivity. Results identify lines 65-68, 38-65, and 8-5 as the most critical N-1 contingencies, while the combined outage of 65-68 and 23-24 gives the most severe N-2 case. FFT energy shows strong rank consistency with angle-deviation severity and complements LOI and L-index indicators. The SVM achieves 83.18% accuracy on a grouped holdout of unseen contingencies and 83.06% under grouped K-fold cross-validation. Stochastic renewable and ramp-event analyses show corridor-dependent severity changes. Scalability tests demonstrate practical screening capability while indicating the need for filtering and parallelization in very large systems.

This is an open access article under the CC BY-SA license.

Corresponding Author:

Indar Chaerah Gunadin
Department of Electrical Engineering, Faculty of Engineering, Universitas Hasanuddin
Perintis Kemerdekaan St. Km. 10, Makassar 90222, Indonesia
Email: indar@eng.unhas.ac.id

1. INTRODUCTION

The increasing penetration of renewable energy resources has changed the operational characteristics of modern power systems. Conventional grids dominated by synchronous generators are being transformed into renewable-rich and inverter-interfaced networks, where photovoltaic (PV) and wind generation introduce variability, uncertainty, reduced inertia, and new stability challenges [1]–[4]. Operating experience with high levels of variable and inverter-based resources further indicates that renewable integration can alter frequency response, voltage behavior, generation dispatch, and transmission power-flow patterns [5]–[8]. These changes make fast and reliable contingency screening increasingly important for renewable-integrated transmission systems.

Static contingency assessment is commonly performed using alternating current (AC) power flow because it represents voltage magnitude, reactive power, nonlinear losses, and branch apparent power. However, repeated AC-based N-1 and N-2 evaluations can be computationally demanding when many outages and operating scenarios must be examined. Reviews of static-security assessment, standard test systems, transmission contingencies, and power-flow-based vulnerability analysis show that simplified screening methods are still required to reduce the number of cases requiring detailed AC evaluation [9]–[12]. Direct current (DC) load flow provides a computationally efficient alternative for preliminary screening, but

it neglects line resistance, reactive power, voltage-magnitude variation, and nonlinear losses. Therefore, DC analysis should be used for candidate prioritization rather than as a complete replacement for AC power flow.

Recent studies have extended contingency assessment through stochastic load flow, SVM-based classification, renewable-energy resilience analysis, voltage-stability prediction, wind-uncertainty indices, and renewable-integrated contingency evaluation [13]–[18]. Deep-learning feature extraction, security classification, renewable-aware N-1 assessment, topology-robust evaluation, and scalable rare-event risk analysis have also demonstrated the potential of data-driven methods to accelerate power-system security assessment [19]–[23]. Nevertheless, three gaps remain. First, many studies emphasize either physical security indices or data-driven classifiers separately, which can reduce operator interpretability. Second, machine-learning performance may be optimistic when highly correlated branch samples from the same contingency and operating scenario are distributed across both training and testing sets. Third, limited work has integrated rapid DC screening, case-by-case AC validation, spatial spectral characterization, leakage-controlled classification, stochastic renewable analysis, scalability evaluation, and EMS-oriented decision support within one reproducible framework.

To address these gaps, this study proposes an integrated static-security screening framework for renewable-integrated transmission systems. The framework combines DC-load-flow-based N-1/N-2 screening, AC power-flow validation, fast Fourier transform (FFT) spatial spectral feature extraction, and support vector machine (SVM) classification. FFT is not interpreted as a temporal electromechanical oscillation metric. Instead, it is used as a spatial spectral transformation of post-contingency bus-angle-deviation patterns under a fixed IEEE 118-bus ordering. The DC model serves as a fast preliminary screening engine, while AC power flow provides the reference for evaluating voltage, reactive power, branch-loading, and nonlinear effects.

The main contributions of this study are as follows: i) A reproducible MATLAB/MATPOWER-based contingency-assessment framework is developed for an IEEE 118-bus system integrated with a 50 MW PV unit and an 80 MW wind unit; ii) DC screening is evaluated against AC power flow using case-by-case error analysis, line-resistance sensitivity, and reactive-load sensitivity; iii) FFT-based spatial spectral features are benchmarked against the line overload index (LOI) and L-index voltage-stability indicator; iv) SVM classification is evaluated using grouped holdout testing on unseen contingency-scenario groups and grouped K-fold cross-validation; and v) Stochastic renewable variability, ramp events, supplementary dynamic screening, large-system scalability testing, and EMS-oriented corrective-action mapping are incorporated to improve operational relevance.

The proposed framework is intended to support early-stage contingency prioritization rather than replace detailed AC, transient-stability, or electromagnetic-transient studies. By combining fast physical screening, complementary spectral information, leakage-controlled machine-learning validation, and operator-oriented outputs, the framework can support contingency monitoring, corrective redispatch planning, topology-reconfiguration assessment, voltage-support review, and controlled load-shedding preparation in renewable-integrated transmission networks.

2. METHOD

This study develops a framework for static-security contingency screening in a renewable-integrated transmission network. The framework combines DC-based N-1/N-2 screening, AC validation, FFT-based spatial spectral features, conventional-index benchmarking, stochastic renewable scenarios, leakage-controlled SVM classification, supplementary dynamic screening, scalability testing, and EMS-oriented decision support. DC load flow is used only as a fast preliminary screening engine, whereas AC power flow remains the reference for voltage magnitude, reactive power, branch apparent power, and validation. The simulations were implemented in MATLAB. All computations were performed on an ASUS ROG Strix G512LI laptop equipped with an Intel Core i7-10750H processor at 2.60 GHz (6 cores and 12 logical processors), 32 GB RAM, an NVIDIA GeForce GTX 1650 Ti with 4 GB VRAM, and Windows 11 Home Single Language 64-bit.

2.1. Simulation system and workflow

The study uses the MATPOWER IEEE 118-bus benchmark, which contains 118 buses, 186 transmission branches, and 54 existing generator records. A 50 MW photovoltaic unit is added at Bus 30 and an 80 MW wind unit at Bus 40, giving 56 generator records in the modified case. The renewable units are represented as generator injections with active-power limits of 0-50 MW and 0-80 MW, voltage set points of 1.0 p.u., and reactive-power limits of ±30 MVar and ±40 MVar, respectively. These capacities were selected as moderate injections that produce measurable power-flow redistribution without replacing the original generation portfolio or altering the benchmark topology. Three deterministic renewable operating conditions are evaluated: Normal (100% of the rated PV and wind outputs), 50% derating, and Outage (0% renewable

output). For each operating condition, separate AC and DC base cases are solved so that every post-contingency state is compared with the base state of the same renewable scenario. The AC reference uses the Newton-Raphson algorithm, whereas the DC model is used for rapid contingency enumeration.

The workflow comprises: system construction; base-case AC/DC solution; full N-1 and top-K N-2 screening; AC validation of severe cases; FFT spatial-feature extraction; LOI and L-index benchmarking; deterministic, Monte Carlo, and ramp-event analysis; grouped SVM validation; simplified converter-oriented dynamic screening; large-system scalability testing; and EMS-oriented corrective-action mapping. Figure 1 summarizes the complete workflow, and Figure 2 presents the modified network. Recent studies have demonstrated static-security assessment for large power systems under single and sequential contingency conditions [24], [25], while learning-based N-1/N-2 screening has also been applied to practical large-scale networks [26]. Open benchmark datasets and simulation engines further support reproducible power-system research [27].

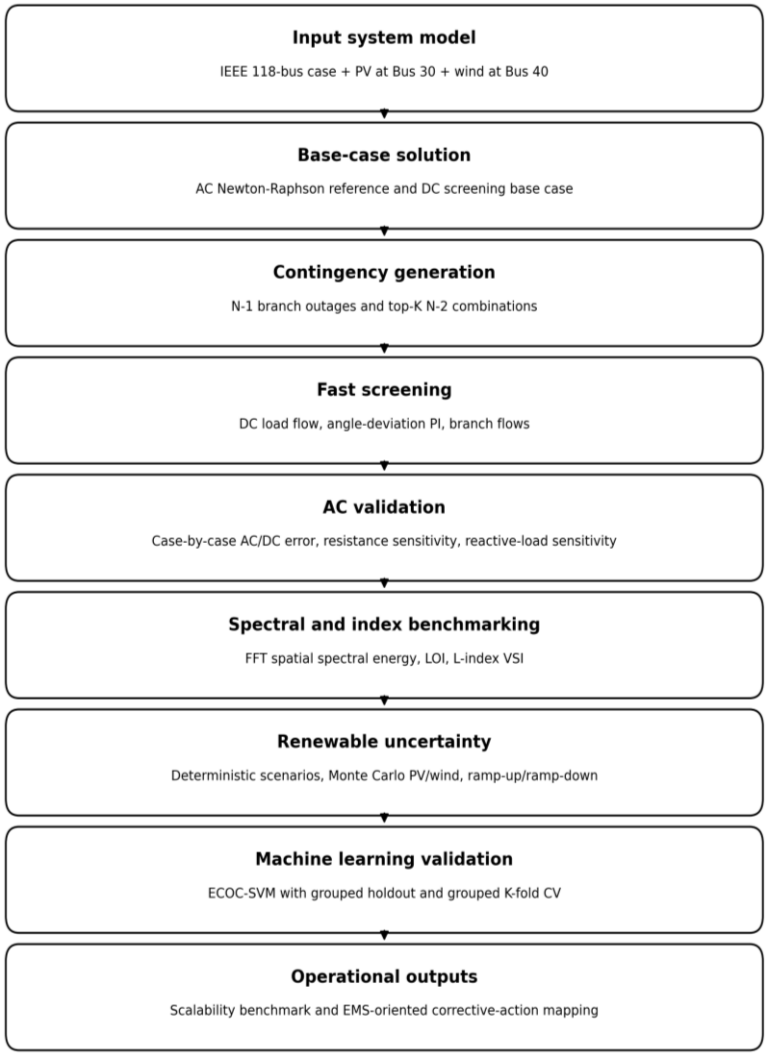

Figure 1. Overall workflow of the proposed static-security contingency screening framework

2.2. AC/DC screening, ratings, and security labels

AC Newton-Raphson power flow is used as the reference because it captures voltage magnitude, reactive power, nonlinear network behavior, and branch apparent power. DC load flow assumes near-unity voltage magnitudes, small angle differences, negligible resistance, and no reactive power. Its active-power balance is expressed as $P = B\theta$, where P is the vector of net bus active-power injections, B is the bus-susceptance matrix, and θ is the bus-angle vector.

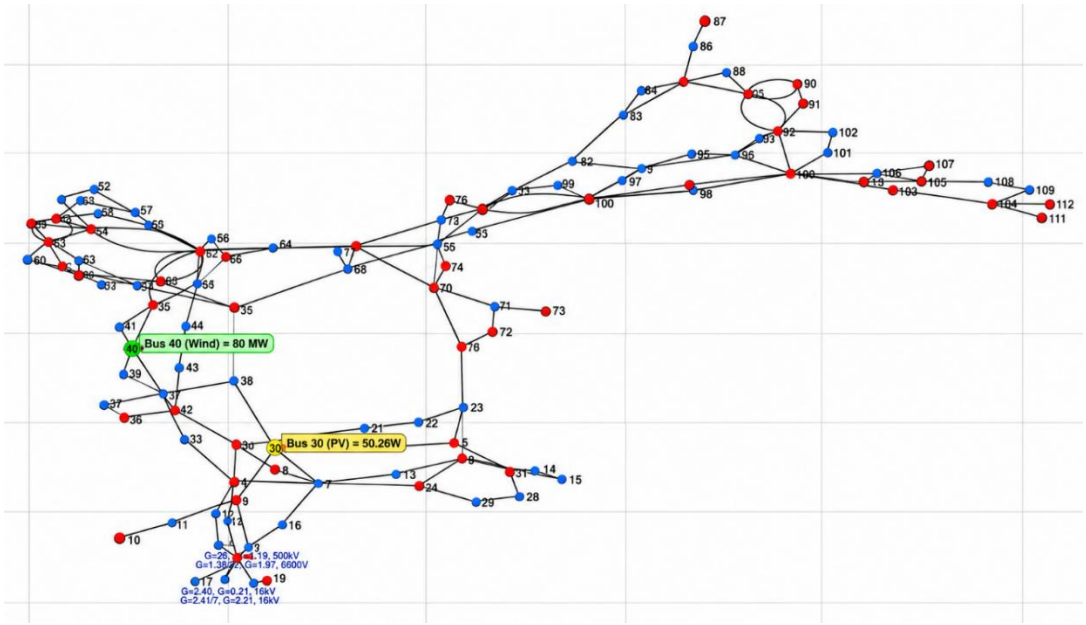

Figure 2. Modified IEEE 118-bus network with PV and wind integration. The PV unit is connected at Bus 30, and the wind unit is connected at Bus 40

Because several MATPOWER RATE_A entries are zero or represent unconstrained limits, a finite effective rating is required for comparative loading and class-label calculation. Original ratings are retained when 0 < RATE_A < 9000 MVA. Otherwise, the effective rating is derived from base-case AC apparent flow:

$$S_{ij}^{\max,\text{eff}} = \max\left(1.25 S_{ij}^{\text{base}}, 50\right) \quad (1)$$

where S^{base}_{ij} is the larger of the from-end and to-end apparent powers of branch i-j in the AC base case. The derived values are used only as reproducible screening ratings and are not interpreted as actual utility protection or emergency limits.

For N-1 analysis, each of the 186 branches is removed individually. The ten most severe converged N-1 cases are then paired, producing up to 45 top-K N-2 candidates. Contingency severity is ranked using the total absolute post-contingency angle deviation:

$$PI_\theta = \sum_{i=1}^{N_b} \left|\theta_i^{\text{post}} - \theta_i^{\text{base}}\right| \quad (2)$$

where N_b is the number of buses and the angles are expressed in degrees. Branch apparent power is evaluated at both ends, $S_{ij} = \max\left\{\sqrt{P_f^2 + Q_f^2}, \sqrt{P_t^2 + Q_t^2}\right\}$, and the AC loading percentage is:

$$\text{Loading}_{ij} = \left(\frac{S_{ij}}{S_{ij}^{\max,\text{eff}}}\right) \times 100\% \quad (3)$$

Branch states are labeled safe for loading below 80%, unsafe for loading from 80% to 100%, and critical for loading above 100%. These AC-derived labels are used as SVM targets. AC loading is not used as an SVM predictor, thereby avoiding direct target leakage.

2.3. AC validation and security analysis

The ten most severe N-1 and ten most severe N-2 cases are re-evaluated using AC power flow. The case-by-case validation records AC and DC angle-deviation PI, relative PI error, mean and maximum bus-angle error, mean and maximum active-flow error, minimum voltage magnitude, maximum voltage deviation, maximum reactive flow, computation time, and AC/DC speedup. Relative PI error is calculated as (4).

$$\text{Error}_{PI} = \frac{\left|PI_\theta^{DC} - PI_\theta^{AC}\right|}{\left|PI_\theta^{AC}\right|} \times 100\% \quad (4)$$

Two controlled sensitivity studies quantify the principal limitations of the DC approximation. Branch resistance is scaled by $\alpha_R \in \{0, 0.5, 1.0, 1.5, 2.0\}$, while reactive demand is scaled by $\alpha_Q \in \{0.5, 1.0, 1.5\}$. These tests show how resistive losses, reactive demand, voltage variation, and reactive-flow redistribution affect AC/DC disagreement. The reported errors are comparative validation metrics rather than formal IEEE compliance limits because acceptable voltage and angle tolerances depend on utility-specific operating criteria and network conditions.

2.4. FFT spatial features and conventional-index benchmarking

FFT is applied to the spatial pattern of post-contingency bus-angle deviations and is not interpreted as a temporal oscillation frequency or physical bus identifier. For each contingency, the angle-deviation vector, $\Delta\theta = \theta^{post} - \theta^{base}$, is converted to radians and mean-removed. The original MATPOWER case118 bus ordering is retained; therefore, the spectral coefficients are comparable only under the same bus-ordering convention.

A normalized single-sided spectrum F_k is obtained from the mean-removed angle-deviation vector. Its total spatial spectral energy is calculated as (5):

$$E_{\mathrm{FFT}} = \sum_{k=1}^{K} | F_k |^2 \tag{5}$$

where K is the number of single-sided spectral bins. FFT RMS and the high-frequency ratio are also extracted as normalized descriptors, with the high-frequency region beginning at approximately $0.25\,K$.

For comparison, the line overload index is calculated as (6):

$$\mathrm{LOI} = \sum_{(i,j)\in\mathcal{L}} \left(\frac{S_{ij}}{S_{ij}^{max,eff}}\right)^{2m}, m = 2 \tag{6}$$

where S_{ij} is the branch apparent power and $S_{ij}^{\max,\mathrm{eff}}$ is the effective screening rating. Voltage-stability stress is represented by the maximum L-index [28]:

$$L_{\max} = \max_{j\in\mathcal{D}} \left| 1 - \sum_{i\in\mathcal{G}} F_{ji} \frac{V_i}{V_j} \right| \tag{7}$$

where $\mathcal{G}$ and $\mathcal{D}$ denote generator and load buses, respectively. FFT energy is benchmarked against angle PI, LOI, L-index, and maximum loading using Spearman rank correlation and top-5 overlap. Therefore, FFT is treated as a complementary indicator of global spatial angular stress rather than a replacement for thermal- or voltage-based indices.

2.5. SVM classification and leakage-controlled validation

Each machine-learning sample represents one active branch under a specific contingency and renewable scenario. The predictor vector contains absolute DC active flow, DC loading percentage, branch resistance R, reactance X, impedance magnitude |Z|, DC angle difference across the branch, global angle-deviation PI, FFT RMS, FFT high-frequency ratio, and the mean renewable-output fraction. The target is the AC-derived safe, unsafe, or critical class defined in Section 2.2. A multiclass error-correcting output-code SVM is trained with one-versus-one coding and a radial-basis-function kernel.

$$\mathrm{K}(\mathrm{x_i}, \mathrm{x_j}) = \exp[-\gamma\, ||\mathrm{x_i} - \mathrm{x_j}||^2], \gamma = 1/(2\sigma^2) \tag{8}$$

The model uses standardized predictors, uniform class priors, BoxConstraint $C = 1$, and MATLAB automatic kernel-scale selection for σ. Automatic kernel-scale selection was used after predictor standardization to adapt the RBF width to the dispersion of the heterogeneous input features and to avoid an arbitrary fixed value of γ. To prevent information leakage, all branch samples from the same contingency-scenario case are assigned to one group. A grouped holdout uses 30% of the groups for unseen-contingency testing, while grouped five-fold cross-validation evaluates robustness across all groups. Performance is reported using accuracy, macro precision, macro recall, macro F1-score, class-wise precision, recall, and F1-score, and normalized confusion matrices.

2.6. Supplementary dynamic, scalability, EMS, and reproducibility notes

Renewable uncertainty is evaluated for the five most severe N-1 and five most severe N-2 cases using 100 Monte Carlo samples. PV and wind output fractions are generated from correlated Gaussian

variables with means of 0.70 and 0.75, standard deviations of 0.20 and 0.18, and correlation coefficient 0.35; values are clipped to [0,1]. Quasi-steady ramp-down and ramp-up cases use renewable fractions {1.0, 0.8, 0.6, 0.4, 0.2, 0.0} and the reverse sequence. Each sampled operating point is solved with separate AC and DC base cases before the selected outages are applied. A supplementary linearized electromechanical DC-network model is applied to the two most severe N-1 cases and the most severe N-2 case under normal and renewable-outage conditions. The nominal frequency is 60 Hz, the simulation duration is 10 s, and the output interval is 0.02 s. Conventional generation uses H = 4.0 s and D = 1.0 p.u. Renewable support assumptions are GFL-dominant (H = 0.05 s, D = 0.10 p.u.), Mixed (H = 2.0 s, D = 1.0 p.u.), and GFM-support (H = 4.0 s, D = 2.0 p.u.). The outputs include frequency nadir/zenith, maximum absolute frequency deviation, RoCoF, rotor-angle spread, and settling time. This analysis is only a dynamic-oriented sensitivity screen and does not replace detailed transient-stability or EMT simulation. Scalability is assessed on case118, case300, case1354pegase, case2383wp, and case9241pegase. For each available system, base AC/DC runtimes are measured, and 20 distributed N-1 outages are sampled. The estimated exhaustive N-1 DC time is calculated as the mean sampled outage time multiplied by the number of branches; therefore, this quantity is an estimate rather than a fully enumerated runtime for the largest systems.

EMS-oriented outputs map screening indicators to operator-review actions. Loading above 120% triggers immediate topology-reconfiguration and security-constrained-redispatch assessment, with controlled load shedding prepared only if corrective actions are insufficient; loading of 100-120% triggers corrective redispatch and parallel-path switching review; loading of 80-100% triggers preventive redispatch and enhanced monitoring. Minimum voltage below 0.95 p.u. triggers voltage-support and reactive-reserve review. These outputs are advisory prioritization rules and do not constitute automatic control commands. All data are derived from public benchmark systems; no human participants, animal subjects, or private data are involved. The main reproducibility parameters used throughout the proposed framework are summarized in Table 1, including the renewable operating conditions, contingency settings, sensitivity parameters, SVM validation configuration, and computing platform.

Table 1. Main reproducibility parameters

Parameter	Setting
Random seed	42 (Mersenne Twister)
Base system	MATPOWER case118: 118 buses, 186 branches, 54 original generators
Added renewable units	PV: Bus 30, 50 MW; Wind: Bus 40, 80 MW
Deterministic renewable fractions	1.0, 0.5, and 0.0
N-2 candidate pool	All pairs among the 10 most severe N-1 cases
Derived rating rule	max(1.25 × base AC apparent flow, 50 MVA) when RATE_A is 0 or ≥9000 MVA
Resistance multipliers	{0, 0.5, 1.0, 1.5, 2.0}
Reactive-load multipliers	{0.5, 1.0, 1.5}
Monte Carlo configuration	100 samples; PV $\mu = 0.70$, $\sigma = 0.20$; wind $\mu = 0.75$, $\sigma = 0.18$; $\rho = 0.35$
Ramp fractions	{1.0, 0.8, 0.6, 0.4, 0.2, 0.0} and reverse
SVM configuration	RBF; C = 1; KernelScale = auto; standardization = true; one-vs-one; uniform priors
Grouped validation	30% grouped holdout and 5-fold grouped cross-validation
Dynamic screen	60 Hz; 10 s; 0.02 s output interval
Software and computing platform	MATLAB R2023a; MATPOWER 8.0; Statistics and Machine Learning Toolbox; Intel Core i7-10750H, 32 GB RAM, NVIDIA GTX 1650 Ti 4 GB, Windows 11 64-bit

3. RESULTS AND DISCUSSION

This section presents the results of the proposed static-security screening framework on the renewable-integrated IEEE 118-bus system. The discussion follows a results-to-interpretation structure covering contingency ranking and AC/DC validation, FFT benchmarking and renewable uncertainty, machine-learning robustness, dynamic-oriented screening, scalability, and EMS implications. All findings are interpreted as screening and prioritization outputs; they do not replace full AC security assessment, transient-stability analysis, or electromagnetic-transient validation.

3.1. Contingency ranking and AC/DC validation

Table 2 summarizes the five most severe N-1 and N-2 contingencies ranked by the steady-state angle-deviation performance index (PI). The outage of line 65-68 produces the largest N-1 PI of 705.52 degrees, followed by 38-65 and 8-5. For N-2 screening, the combined outage of 65-68 and 23-24 gives the largest PI of 1585.53 degrees. The repeated appearance of 65-68, 38-65, 23-24, and 8-5 indicates that these branches act as influential transfer paths in the modified network. Their removal forces substantial active-power and voltage-angle redistribution through adjacent corridors rather than merely creating a local disturbance. Figure 3 presents these ranked PI values, with the 65-68 outage and the combined 65-68/23-24 outage producing the highest values among the N-1 and N-2 cases, respectively.

The structural interpretation is supported by the detailed branch-loading results. After the 65-68 outage, loading is transferred toward lines 23-24 and 68-69, which reach approximately 121.03% and 111.20%, respectively. The 38-65 outage shifts stress toward the 42-49, 65-68, and 30-38 paths, while the 8-5 outage produces severe loading on lines 16-17 and 8-30, exceeding 328%. These patterns explain why the same corridors repeatedly appear in the highest-ranked N-1 and N-2 cases: they connect regions whose alternative paths have limited capacity under the adopted screening ratings.

The PI values represent the magnitude of steady-state angular redistribution and should not be interpreted as direct evidence of transient instability. To assess the reliability of the DC ranking, the selected severe cases were re-evaluated using AC power flow. As summarized in Table 3, the relative AC/DC PI error ranges from 9.41% to 51.94%. The error is not uniform in direction: DC analysis overestimates some contingencies and underestimates others because its assumptions neglect resistance, voltage-magnitude variation, reactive flow, and nonlinear losses. Therefore, the DC model is useful for rapid candidate prioritization, but the numerical severity and final operating decision must be confirmed using AC analysis. Figure 4 compares case-by-case AC and DC angle-based severity and the rankings obtained using angle PI, FFT energy, LOI, and L-index.

The resistance sensitivity test provides a direct explanation for the observed disagreement. When branch resistance is removed, AC and DC results are close for the examined cases; increasing the resistance multiplier progressively changes active-flow redistribution and losses, while the DC result remains unchanged. Reactive-load sensitivity produces a different effect: increasing Q demand has a limited influence on DC quantities but reduces the AC minimum voltage and increases voltage deviation. These results confirm that resistance and reactive-power conditions can alter both the magnitude and, in some cases, the ordering of contingency severity. The appropriate operational sequence is therefore DC screening followed by AC validation of the highest-ranked cases.

Table 2. Critical N-1 and N-2 contingency rankings

Rank	Top N-1 outage	PI (degree)	Top N-2 outage	PI (degree)
1	65-68	705.52	65-68, 23-24	1585.53
2	38-65	427.66	65-68, 23-25	984.99
3	8-5	387.43	65-68, 8-5	783.21
4	30-38	258.69	65-68, 30-38	781.25
5	26-30	235.82	30-38, 23-24	738.35

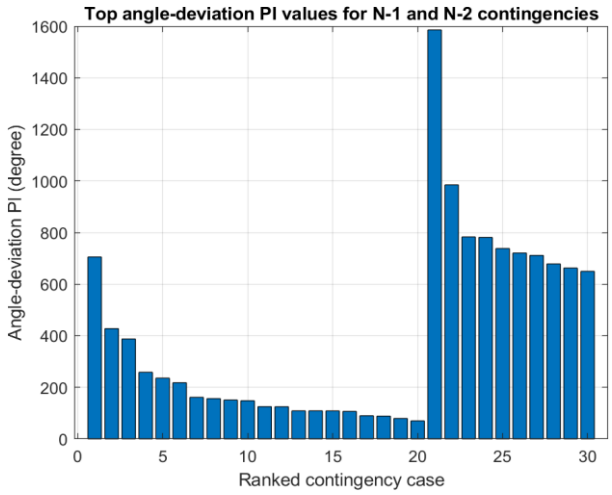

Figure 3. Ranked angle-deviation PI values for the critical N-1 and N-2 contingency cases

Table 3. Compact AC/DC validation and sensitivity findings

Validation aspect	Key result	Interpretation
Case-by-case AC/DC comparison	Relative PI error: 9.41%-51.94%	DC supports ranking, but not final quantitative assessment.
Voltage and reactive-power effects	Minimum voltage: 0.936-0.943 p.u.	Voltage and reactive effects require AC validation.
Resistance sensitivity	65-68 PI error: 3.04% at R=0 to 126.98% at R=2	DC disagreement increases as resistive effects become significant.
Reactive-load sensitivity	Higher Q demand lowers minimum voltage and increases voltage deviation	Reactive stress exposes limitations that are absent from the DC model.

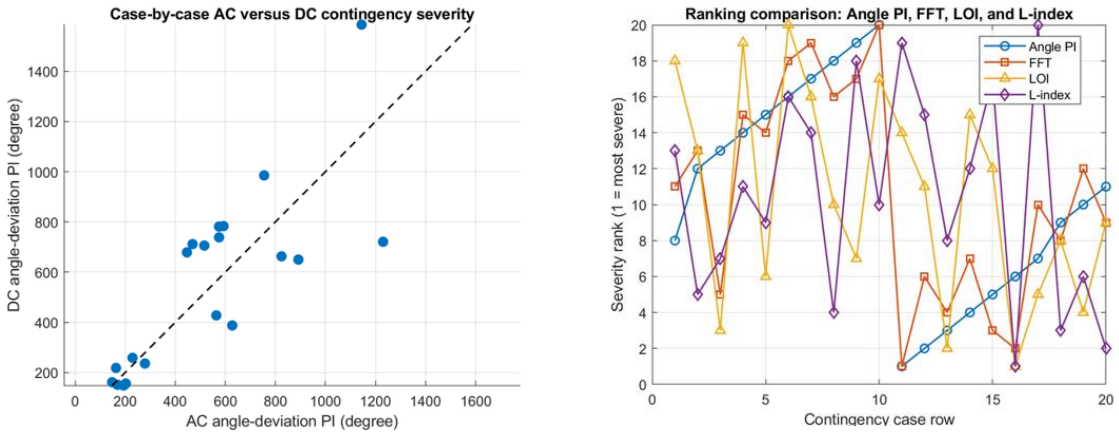

(a) (b)

Figure 4. Comparison of angle-based severity assessment and ranking performance: (a) case-by-case AC/DC angle severity comparison, and (b) ranking comparison among angle PI, FFT energy, LOI, and L-index

3.2. FFT benchmarking and renewable uncertainty

The FFT feature is evaluated as a spatial transformation of the mean-removed post-contingency angle-deviation vector. The spectral-bin index k is neither a bus number nor a temporal oscillation frequency. Its value lies in summarizing how angular stress is distributed across the fixed IEEE 118-bus ordering. Table 4 shows that FFT energy has a strong Spearman rank correlation of 0.883 with angle PI. This agreement indicates that contingencies with broad spatial angle redistribution generally contain greater spectral energy.

FFT should therefore be treated as complementary rather than superior to conventional indices. LOI directly measures thermal loading and achieves complete top-5 agreement with the maximum-loading ranking. By contrast, FFT provides information about the global shape and spatial spread of angle deviations, while the L-index describes voltage-stability stress. The relatively narrow minimum-voltage and L-index variation in the examined cases indicates that thermal and angular redistribution dominate the present static results. Combining these indicators is more informative than relying on any single scalar index. Figure 5 shows the Monte Carlo distribution of DC angle-deviation PI under stochastic PV and wind output, illustrating the variation in contingency severity across the sampled renewable operating conditions.

The stochastic and ramp analyses show that increasing renewable output does not universally improve system security. For the 65-68 contingency, reducing the renewable fraction from 100% to 0% decreases the DC PI from 705.52 to 310.21 degrees. In contrast, the same change increases the PI of 38-65 from 427.66 to 668.37 degrees. The 8-5 case remains almost unchanged, with a PI standard deviation of only 0.59 degrees and loading above 331% across the stochastic samples. Thus, renewable injections do not have a single beneficial or adverse effect. They alter the location and direction of transfer flows, relieving one corridor while increasing stress on another. The N-2 outage of 65-68 and 23-24 is particularly sensitive to renewable uncertainty, with a mean PI of 1333.55 degrees and a standard deviation of 130.05 degrees. This sensitivity suggests that deterministic ranking alone may understate the range of operating severity for contingencies located near major transfer paths. In an EMS context, such cases should receive higher monitoring priority because their severity depends strongly on the current renewable dispatch, whereas persistently critical cases such as 8-5 require preventive action regardless of renewable output.

Table 4. FFT benchmarking and renewable-uncertainty results

Aspect	Result	Main implication
FFT versus angle PI	Spearman correlation = 0.883	FFT is consistent with global angular-stress severity.
FFT versus maximum-loading ranking	Top-5 overlap = 0.60	FFT captures part, but not all, of thermal-overload severity.
LOI versus maximum-loading ranking	Top-5 overlap = 1.00	LOI remains the strongest direct thermal-overload indicator.
Stochastic N-2 case: 65-68, 23-24	Mean PI = 1333.55 deg; standard deviation = 130.05 deg	The case is highly sensitive to renewable variability.
Persistent critical case: 8-5	PI standard deviation = 0.59 deg; worst loading = 331.83%	The contingency remains critical across renewable conditions.
Ramp-event contrast	65-68: 705.52 to 310.21 deg; 38-65: 427.66 to 668.37 deg	Renewable output redistributes stress between corridors.

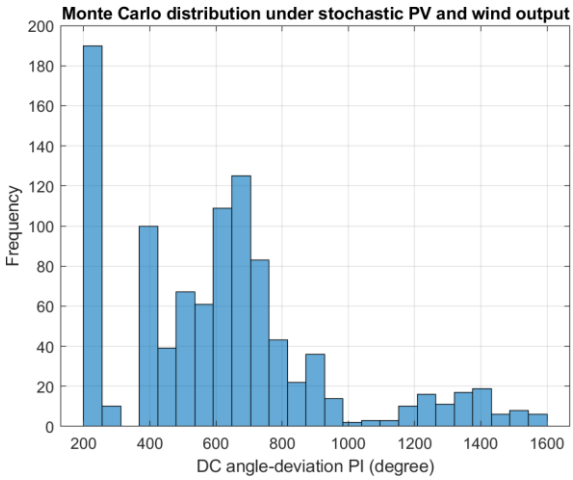

Figure 5. Monte Carlo distribution of DC angle-deviation PI under stochastic PV and wind output

3.3. Machine-learning robustness, dynamic screening, scalability, and EMS implications

The SVM classifier was evaluated using contingency-scenario groups rather than a random branch-level split. Consequently, samples generated from the same outage condition do not appear in both training and testing sets. The grouped holdout achieves 83.18% accuracy, 79.02% macro precision, 83.46% macro recall, and 80.14% macro F1-score. Grouped five-fold cross-validation produces 83.06% accuracy, 77.25% macro precision, 84.22% macro recall, and 79.68% macro F1-score. These results provide a conservative and more credible estimate of generalization to unseen contingencies. Table 5 consolidates the SVM, dynamic-screening, and scalability results, including grouped-validation performance, critical-class detection, the maximum rotor-angle spread, and estimated screening times for the smallest and largest benchmark systems.

At the class level, the grouped holdout precision, recall, and F1-score were 0.961, 0.822, and 0.886 for safe; 0.585, 0.868, and 0.699 for unsafe; and 0.824, 0.814, and 0.819 for critical, respectively. Under grouped five-fold cross-validation, the corresponding precision, recall, and F1-score were 0.960, 0.821, and 0.885 for safe; 0.592, 0.856, and 0.700 for unsafe; and 0.765, 0.849, and 0.805 for critical. The comparatively lower precision of the Unsafe class indicates that most residual errors occur near the 80% and 100% loading boundaries, consistent with the normalized confusion matrices in Figure 6.

The confusion matrices are dominated by diagonal entries. Most remaining errors occur between adjacent severity classes: safe versus unsafe and unsafe versus critical. This pattern is expected because the labels are separated by fixed 80% and 100% loading thresholds, so observations close to a boundary can change class after relatively small AC/DC discrepancies. Importantly, the Critical class retains F1-scores of 0.819 in holdout testing and 0.805 in grouped cross-validation. The classifier is therefore suitable as an early-warning assistant, but it should not replace physics-based confirmation for switching or load-shedding decisions. The supplementary dynamic-oriented analysis reports small center-of-inertia frequency deviations but a maximum rotor-angle spread of approximately 82.71 degrees for the most severe N-2 case. The small frequency excursion is consistent with the simulated disturbance type, which is a transmission outage rather than a major generation-loss event. Rotor-angle spread is consequently the more informative output in this simplified model. Differences among grid-following-dominant, mixed, and grid-forming-support assumptions are interpreted only as sensitivity indicators because detailed converter loops, phase-locked loops, governors, exciters, protection systems, and EMT phenomena are not represented.

Table 5. SVM, dynamic-screening, and scalability results

Evaluation item	Result	Interpretation
Grouped holdout on unseen contingencies	Accuracy = 83.18%; macro F1 = 80.14%	Realistic performance without contingency-level leakage.
Grouped five-fold cross-validation	Accuracy = 83.06%; macro F1 = 79.68%	Performance is stable across grouped folds.
Critical-class detection	F1 = 0.819 (holdout); 0.805 (CV)	Critical states remain detectable with acceptable reliability.
Dynamic-oriented screening	Maximum rotor-angle spread = 82.71 deg for 65-68, 23-24	Supplementary linearized indicator, not EMT validation.
Scalability: case118	Estimated full N-1 DC time = 5.82 s	Fast sequential screening is feasible on the study system.
Scalability: case9241pegase	Estimated full N-1 DC time = 1508.92 s	Large systems require filtering, parallelization, or distributed execution.

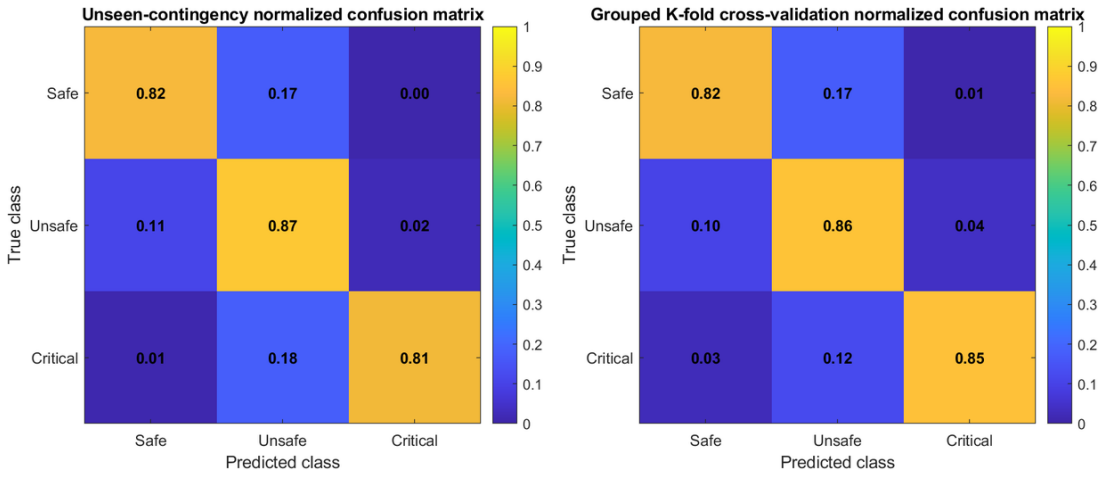

Figure 6. Normalized confusion matrices for unseen-contingency holdout and grouped K-fold validation

The scalability benchmark shows that estimated full sequential N-1 DC screening increases from 5.82 s for case118 to 1508.92 s for case9241pegase. This result supports computational feasibility but also defines the practical boundary of the current implementation. For national-scale applications, the framework should use pre-contingency filtering, parallel branch evaluation, distributed computation, and selective AC escalation. The scalability result should therefore be interpreted as evidence of extensibility, not as proof that the unmodified sequential implementation is already suitable for sub-second real-time operation. The EMS-oriented output converts screening indicators into advisory actions. Contingencies with moderate loading can be assigned to enhanced monitoring or preventive redispatch. Cases with loading above 100% require security-constrained redispatch, evaluation of alternative transfer paths, and topology-reconfiguration assessment. When overload coincides with reduced voltage margin, reactive support and voltage-control resources should also be reviewed. For extreme cases such as the N-1 outage of 8–5 and the combined N-2 outage of 38–65 and 8–5, controlled load shedding is considered only if redispatch, topology changes, and voltage-support actions are insufficient.

3.4. Integrated discussion and limitations

Compared with previous contingency-filtering, vulnerability-index, stochastic, hybrid AC/DC, and machine-learning studies [9]–[15], [21]–[26], the contribution of this work is not a new physical stability law or a new learning algorithm. Its novelty lies in the integration and validation sequence: rapid DC N-1/N-2 screening, case-by-case AC verification, resistance and reactive-load sensitivity, spatial FFT characterization, conventional-index benchmarking, grouped unseen-contingency SVM evaluation, stochastic renewable analysis, large-system scalability testing, and EMS-oriented action mapping within one reproducible pipeline. This integrated design provides greater operational transparency than a standalone black-box classifier and broader stress characterization than a single overload or voltage index. The results also clarify the role of each component. DC load flow supplies speed, AC power flow supplies physical confirmation of voltage and reactive effects, LOI identifies direct thermal stress, FFT characterizes the spatial distribution of angular deviations, and SVM converts multiple physical and spectral features into branch-level warning classes. No component is universally superior; their value arises from complementary use. This positioning is more defensible than claiming that FFT alone improves stability assessment or that SVM replaces established power-system analysis.

Several limitations remain: i) The study is simulation-based and has not been validated using utility SCADA, PMU, or disturbance records; ii) The 50 MW PV and 80 MW wind units represent a moderate renewable modification and do not reproduce a 30%-40% system-wide renewable replacement scenario; iii) PV and wind are modeled as simplified injections rather than detailed converter-control systems; iv) FFT coefficients depend on the fixed MATPOWER case118 bus ordering and cannot be compared after arbitrary bus relabeling; v) The top-K N-2 strategy may miss an uncommon severe pair formed from lower-ranked N-1 outages; vi) Missing or unconstrained RATE_A values are replaced with derived screening ratings; therefore, the reported loading percentages are comparative indicators rather than actual utility protection limits; finally, vii) The dynamic analysis is linearized, and the scalability times are based partly on sampled-outage extrapolation. These limitations define the framework as a reproducible screening baseline that should be followed by detailed AC, transient, EMT, and utility-specific studies before deployment.

4. CONCLUSION

This study developed a compact and reproducible static-security screening framework for contingency assessment in a renewable-integrated IEEE 118-bus system. The framework combines DC load-flow-based N-1/N-2 screening, AC validation, FFT-based spatial spectral feature extraction, traditional index benchmarking, leakage-controlled SVM classification, stochastic renewable analysis, scalability testing, and EMS-oriented decision support. The results identify line 65-68 as the most severe N-1 contingency with an angle-deviation PI of 705.52°, while the combined outage of 65-68 and 23-24 is the most severe N-2 case with a PI of 1585.53°. Case-by-case AC/DC validation shows that DC load flow is useful for fast screening, but its error is contingency-dependent; therefore, the proposed framework should be used as a prioritization tool rather than a complete substitute for AC power-flow analysis. The analysis also clarifies the respective roles of FFT and SVM.

FFT energy is used as a spatial spectral indicator of post-contingency angle-deviation patterns and complements, but does not replace, LOI and L-index indicators. The leakage-controlled SVM evaluation provides a more realistic robustness estimate, achieving 83.18% accuracy on unseen-contingency grouped holdout and 83.06% accuracy using grouped K-fold cross-validation. Stochastic renewable and ramp-event results further show that renewable variability affects contingency severity in a corridor-dependent manner rather than producing a universal improvement or degradation. Scalability and EMS mapping indicate that the framework can support operator-oriented contingency prioritization, corrective redispatch planning, topology review, voltage-support assessment, and controlled load-shedding preparation. The main limitations are the simplified PV and wind injection models, the dependence of FFT features on the fixed IEEE 118-bus ordering, the use of derived screening ratings for branches with missing or unconstrained thermal limits, and the simplified linearized dynamic/converter-oriented screening. Future work will extend the framework using detailed grid-forming and grid-following converter models, measured renewable profiles, parallelized large-scale contingency enumeration, comparative evaluation against long short-term memory (LSTM) and graph-neural-network models, real utility network data, and EMS/SCADA integration.

ACKNOWLEDGMENTS

The author wishes to express gratitude to the members of the Relay and Measurement Laboratory at Hasanuddin University for their support and help during the completion of this study.

FUNDING INFORMATION

The authors declare that this research received no external funding.

AUTHOR CONTRIBUTIONS STATEMENT

This journal uses the Contributor Roles Taxonomy (CRediT) to recognize individual author contributions, reduce authorship disputes, and facilitate collaboration.

Name of Author	C	M	So	Va	Fo	I	R	D	O	E	Vi	Su	P	Fu
Yusri Ambabunga	✓	✓	✓	✓	✓	✓		✓	✓		✓		✓	
Indar Chaerah Gunadin	✓	✓		✓	✓		✓			✓		✓		
Yusri Syam Akil		✓		✓	✓		✓			✓		✓		
Zaenab Muslimin				✓	✓	✓	✓			✓		✓		

C : **C**onceptualization
M : **M**ethodology
So : **So**ftware
Va : **Va**lidation
Fo : **Fo**rmal analysis
I : **I**nvestigation
R : **R**esources
D : **D**ata Curation
O : Writing - **O**riginal Draft
E : Writing - Review & **E**diting
Vi : **Vi**sualization
Su : **Su**pervision
P : **P**roject administration
Fu : **Fu**nding acquisition

CONFLICT OF INTEREST STATEMENT

The authors declare that they have no known competing financial interests or personal relationships that could have appeared to influence the work reported in this paper.

DATA AVAILABILITY

The benchmark power system data used in this study (IEEE 118-bus system) are publicly available. The derived data generated from simulations, including contingency results, spectral indices, and classification outputs, are available from the corresponding author upon reasonable request.

REFERENCES

[1] Y. Yang, Y. Wen, Z. Zhang, Y. Dong, C. Shen, and Y. Liu, "Toward 100% renewable power grids: a review," *IEEE Access*, vol. 13, pp. 69690–69704, 2025, doi: 10.1109/ACCESS.2025.3558772.

[2] A. Poulose and S. Kim, "Transient stability analysis and enhancement techniques of renewable-rich power grids," *Energies*, vol. 16, no. 5, Mar. 2023, doi: 10.3390/en16052495.

[3] M.-T. Kuo, "Optimized energy storage integration for enhancing grid stability under high photovoltaic penetration scenarios," in *2025 IEEE Industry Applications Society Annual Meeting (IAS)*, Jun. 2025, pp. 1–8, doi: 10.1109/IAS62731.2025.11061737.

[4] N. Zhang *et al.*, "Data-driven security and stability rule in high renewable penetrated power system operation," *Proceedings of the IEEE*, vol. 111, no. 7, pp. 788–805, Jul. 2023, doi: 10.1109/JPROC.2022.3192719.

[5] M. Negnevitsky, "High renewable energy penetration and power system security: New challenges and opportunities," *Proceedings of the 10th International Scientific Symposium on Electrical Power Engineering, ELEKTROENERGETIKA 2019*, pp. 16–25, 2019.

[6] D. Lew *et al.*, "Getting to 100% renewables: operating experiences with very high penetrations of variable energy resources," *IET Renewable Power Generation*, vol. 14, no. 19, pp. 3899–3907, Dec. 2020, doi: 10.1049/iet-rpg.2020.0573.

[7] A. Hoke, V. Gevorgian, S. Shah, P. Koralewicz, R. W. Kenyon, and B. Kroposki, "Island power systems with high levels of inverter-based resources: stability and reliability challenges," *IEEE Electrification Magazine*, vol. 9, no. 1, pp. 74–91, Mar. 2021, doi: 10.1109/MELE.2020.3047169.

[8] S. Rahman *et al.*, "Analysis of power grid voltage stability with high penetration of solar PV systems," *IEEE Transactions on Industry Applications*, vol. 57, no. 3, pp. 2245–2257, May 2021, doi: 10.1109/TIA.2021.3066326.

[9] E. A. Hailu, G. N. Nyakoe, and C. M. Muriithi, "Techniques of power system static security assessment and improvement: a literature survey," *Heliyon*, vol. 9, no. 3, Mar. 2023, doi: 10.1016/j.heliyon.2023.e14524.

[10] S. Peyghami, P. Davari, M. Fotuhi-Firuzabad, and F. Blaabjerg, "Standard test systems for modern power system analysis: an overview," *IEEE Industrial Electronics Magazine*, vol. 13, no. 4, pp. 86–105, Dec. 2019, doi: 10.1109/MIE.2019.2942376.

[11] J. Giri, S. R. Chauhan, and S. N. Mishra, "Review on contingency and its effects in transmission lines," *SMART MOVES JOURNAL IJOSCIENCE*, pp. 56–60, Jan. 2021, doi: 10.24113/ijoscience.v7i1.385.

[12] A. Abedi, L. Gaudard, and F. Romerio, "Power flow-based approaches to assess vulnerability, reliability, and contingency of the power systems: The benefits and limitations," *Reliability Engineering & System Safety*, vol. 201, Sep. 2020, doi: 10.1016/j.ress.2020.106961.

[13] N. Gupta, "Stochastic load flow method for contingency analysis of power systems," in *2021 IEEE 2nd International Conference on Smart Technologies for Power, Energy and Control (STPEC)*, Dec. 2021, pp. 1–6, doi: 10.1109/STPEC52385.2021.9718747.

[14] M. S, S. B. Daram, S. K. S, and D. R, "Predictive modeling of power system contingencies with SVMs and FACTS devices for enhanced stability," *International Journal of Electrical and Electronics Engineering*, vol. 10, no. 9, pp. 112–123, Sep. 2023, doi: 10.14445/23488379/IJEEE-V10I9P111.

[15] A. Kumar, Y. R. Sood, and A. Maheshwari, "Enhancing power system resilience: a contingency-based approach for integrating renewable energy sources," in *2023 Second IEEE International Conference on Measurement, Instrumentation, Control and Automation (ICMICA)*, May 2024, pp. 1–6, doi: 10.1109/ICMICA61068.2024.10732463.

[16] M. J. Abbass, R. Lis, and W. Rebizant, "Advanced voltage stability assessment in renewable-powered islanded microgrids using machine learning models," *Energies*, vol. 18, no. 8, Apr. 2025, doi: 10.3390/en18082047.

[17] S. R. Pani and R. K. Samal, "Evaluation of power grid vulnerability indices accounting for wind power uncertainty," *Sustainable Energy, Grids and Networks*, vol. 38, Jun. 2024, doi: 10.1016/j.segan.2024.101354.

[18] R. S. Waghmare, S. Bhat, and B. K. Dora, "Contingency analysis of IEEE 14 bus system with integration of DFIG wind farm," in *2024 IEEE 4th International Conference on Sustainable Energy and Future Electric Transportation (SEFET)*, Jul. 2024, pp. 1–5, doi: 10.1109/SEFET61574.2024.10718099.

[19] M. Sun, I. Konstantelos, and G. Strbac, "A deep learning-based feature extraction framework for system security assessment," *IEEE Transactions on Smart Grid*, vol. 10, no. 5, pp. 5007–5020, Sep. 2019, doi: 10.1109/TSG.2018.2873001.

[20] J.-M. H. Arteaga, F. Hancharou, F. Thams, and S. Chatzivasileiadis, "Deep learning for power system security assessment," in *2019 IEEE Milan PowerTech*, Jun. 2019, pp. 1–6, doi: 10.1109/PTC.2019.8810906.

[21] T. Qian *et al.*, "N-1 static security assessment method for power grids with high penetration rate of renewable energy generation," *Electric Power Systems Research*, vol. 211, Oct. 2022, doi: 10.1016/j.epsr.2022.108200.

[22] A. King and S. Grijalva, "A deep learning framework for robust N-1 power system security evaluation considering renewable energy generation and topological variation," in *2025 Cyber Awareness and Research Symposium (CARS)*, Oct. 2025, pp. 1–9, doi: 10.1109/CARS67163.2025.11337421.

[23] B. Tan, J. Zhao, and Y. Chen, "Scalable risk assessment of rare events in power systems with uncertain wind generation and loads," *IEEE Transactions on Power Systems*, vol. 40, no. 2, pp. 1374–1388, Mar. 2025, doi: 10.1109/TPWRS.2024.3435490.

[24] P. Sai Nandini, R. Krishan, and D. Pullaguram, "Static security assessment of large power systems under contingency cases," in *2022 IEEE 10th Power India International Conference (PIICON)*, Nov. 2022, pp. 1–6, doi: 10.1109/PIICON56320.2022.10045158.

[25] P. S. V Prabhakar, R. Krishan, and D. R. Pullaguram, "Static security assessment of large power systems under N-1-1 contingency," in *2022 22nd National Power Systems Conference (NPSC)*, Dec. 2022, pp. 35–40, doi: 10.1109/NPSC57038.2022.10069705.

[26] I. Priyadi *et al.*, "Enhancing power system security through deep CNN-based N-1 and N-2 contingency screening: application in Indonesia's Java-Madura-Bali Grid Network," *International Review of Electrical Engineering (IREE)*, vol. 20, no. 3, Jun. 2025, doi: 10.15866/iree.v20i3.26115.

[27] I. Aravena *et al*., "Open power system datasets and open simulation engines: a survey toward machine learning applications," *IEEE Open Access Journal of Power and Energy*, vol. 12, pp. 353–365, 2025, doi: 10.1109/OAJPE.2025.3573958.
[28] H. S. Salama and I. Vokony, "Voltage stability indices–A comparison and a review," *Computers and Electrical Engineering*, vol. 98, Mar. 2022, doi: 10.1016/j.compeleceng.2022.107743.

BIOGRAPHIES OF AUTHORS



Yusri Ambabunga was born in Ujung Pandang, South Sulawesi, Indonesia. He received his bachelor's degree in electrical engineering from Atma Jaya Catholic University of Makassar, South Sulawesi, Indonesia. He subsequently obtained his master's degree in electrical engineering from Universitas Hasanuddin, Makassar, South Sulawesi, Indonesia. He is currently pursuing a doctoral degree in electrical engineering at Universitas Hasanuddin and is in the coursework and dissertation preparation stages. He can be contacted at email: ambabungayam21d@student.unhas.ac.id.



Indar Chaerah Gunadin was born in Palopo, South Sulawesi, Indonesia. He received his bachelor's degree in electrical power engineering from Universitas Hasanuddin, Makassar, Indonesia, in 1997. He subsequently obtained his master's and Ph.D. degrees from Institut Teknologi Sepuluh Nopember, Indonesia, in 2006 and 2013, respectively. He is a professor in the Department of Electrical Engineering at Universitas Hasanuddin and currently serves as the head of the Relay, Protection, and Control Laboratory. His research interests include power system stability, flexible AC transmission systems (FACTS) devices, artificial intelligence, and control systems. He is a member of the Indonesian Engineers Union, the Indonesian Electrical Engineering Higher Education Forum, and the Indonesian Electrical Engineering Experts Association. He can be contacted at email: indar@eng.unhas.ac.id.



Yusri Syam Akil was born in Sengkang, South Sulawesi, Indonesia. He received his Ph.D. degree in computer science and electrical engineering from Kumamoto University, Japan, in 2013. He is a professor in the Department of Electrical Engineering at Hasanuddin University, Indonesia. He currently serves as the head of the Energy Efficiency and Conservation Research Group at the same university. His research interests include energy management, power demand analysis and forecasting, and power system optimization. He can be contacted at email: yusakil@unhas.ac.id.



Zaenab Muslimin was born in Ujung Pandang, South Sulawesi, Indonesia. She received her bachelor's, master's, and doctoral degrees from Universitas Hasanuddin, Makassar, Indonesia, in 1990, 2004, and 2021, respectively, with a major in electrical power engineering. She is currently a lecturer in the Department of Electrical Engineering at Universitas Hasanuddin. Her research interests include power system protection and measurement. She is also an active member of the Indonesian Engineers Union. She can be contacted at email: zaenab@unhas.ac.id.